

Constraints on hot metals in the vicinity of the Galaxy

B. McKernan,¹* T. Yaqoob^{2,3} and C. S. Reynolds¹

¹*Department of Astronomy, University of Maryland, College Park, MD 20742, USA*

²*Department of Physics and Astronomy, Johns Hopkins University, Baltimore, MD 21218, USA*

³*Laboratory for High-energy Astrophysics, NASA/Goddard Space Flight Center, Greenbelt, MD 20771, USA*

Accepted 2005 June 2. Received 2005 May 20; in original form 2005 April 8

ABSTRACT

We have searched for evidence of soft X-ray absorption by hot metals in the vicinity of the Galaxy in the spectra of a small sample of 15 type I active galactic nuclei (AGN) observed with the high-resolution X-ray gratings on board *Chandra*. This is an extension of our previous survey of hot O VII and O VIII absorbing gas in the vicinity of the Galaxy. The strongest absorption signatures within a few hundred km s⁻¹ of their rest-frame energies are most likely to be due to warm absorbing outflows from the nearest AGN, which are back-lighting the local hot gas. We emphasize that absorption signatures in the spectra of some distant AGN that are kinematically consistent with the recessional velocity of the AGN are most likely to be due to hot local gas. Along the sightline towards PG 1211+143, PDS 456 and MCG-6-30-15 there is a very large absorbing Fe column density which is kinematically consistent with absorption by hot, local Fe. The sightlines to these three AGN pass through the limb of the Northern Polar Spur (NPS), a local bubble formed from several supernovae which, if rich in Fe, may account for a large local Fe column.

We obtain limits on the column density of local, highly ionized N, Ne, Mg, Si along all of the sightlines in our sample. We correlate the column density limits with those of highly ionized O along the same sightlines. Assuming the hot local gas is in collisionally ionized equilibrium, we obtain limits on the temperature and relative abundances of the metals in the hot local gas. Our limits on the ionic column densities in the local hot gas seem to be consistent with those observed in the hot halo gas of edge-on normal spiral galaxies.

Key words: techniques: spectroscopic – Galaxy: halo – galaxies: active – intergalactic medium – galaxies: Seyfert – X-rays: galaxies.

1 INTRODUCTION

Present-day structures such as galaxies and clusters of galaxies are believed to have condensed from within partially collapsing filaments of primordial matter. The legacy of the structure formation epoch includes shock-heated filaments as well as structures and these filaments should thread the modern universe. Simulations of structure formation indicate that around half of the baryonic matter at low redshift lives in such filaments, shock-heated to $\sim 10^{5-7}$ K (see, e.g., Cen & Ostriker 1999; Davé et al. 2001 and references therein). Although more recent work by Kang et al. (2005) suggests that a lower-temperature component ($T < 10^5$ K) of the shock-heated filaments may be more significant than previously thought. The ‘warm’ ($\sim 10^{5-6}$ K) component of this warm/hot intergalactic medium (WHIGM) has been observed in absorption in the ultraviolet (UV) band (see, e.g., Tripp, Savage & Jenkins 2000 and references therein). However, much of the WHIGM is expected to

be hotter than this, so the high spectral resolution X-ray detectors such as those aboard *Chandra* and *XMM-Newton* are best placed for investigating the ‘hot’ component of the missing baryons.

The clearest X-ray spectral signature of hot gas in the vicinity of our Galaxy consists of absorption features imprinted in spectra of X-ray bright active galactic nuclei (AGN) at $z = 0$ in the observed frame (Hellsten, Gnedin & Miralde-Escudé 1998; Perna & Loeb 1998). One of the most important new results from the *Chandra* and *XMM-Newton* X-ray telescopes, has been the discovery of hot, low-density, highly ionized gas in the vicinity of our Galaxy (at $z = 0$) and possibly beyond (at $z > 0$). X-ray absorption due to local ($z = 0$) hot gas was discovered recently (Cagnoni 2002; Fang et al. 2002; Nicastro et al. 2002; Rasmussen, Kahn & Paerels 2002; Fang, Sembach & Canizares 2003; McKernan et al. 2003a,b; McKernan, Yaqoob & Reynolds 2004). Of course, such absorption need not be due to local WHIGM. Absorption by hot gas at $z = 0$ could be due to local Galactic gaseous structures or infalling high-velocity clouds (see, e.g., Sembach et al. 2003; Collins, Shull & Giroux 2004 and references therein). Even if there are no known local structures along the sightline to a particular AGN, the location of the absorbing

*E-mail: mckernan@astro.umd.edu

gas is still ambiguous. Around half of all type I AGN exhibit strong absorption in the soft X-ray and UV bands due to partially ionized, optically thin, outflowing, circum-nuclear material known as the ‘warm absorber’ (see, e.g., McKernan, Yaqoob & Reynolds 2005 and references therein). Since the warm absorbers are outflowing, absorption which is actually local to our Galaxy at $z \sim 0$ could be misinterpreted as a warm absorber outflow coinciding with the cosmological recession velocity (cz) of the AGN (see, e.g., fig. 3 of McKernan et al. 2004). Confusion with AGN outflow is a worse problem for WHIM at intermediate redshifts ($z > 0$). The few apparently robust detections of absorbers at redshifts intermediate between our Galaxy and the AGN rest-frame, e.g. Nicastro et al. (2005) could be variable (Ravasio et al. 2005), which is suggestive of an origin in an ionized outflow from the host AGN, rather than WHIM.

In this paper, we investigate a sample of AGN observed with the high-energy transmission gratings (Markert et al. 1995) on board *Chandra*. The uniform analysis of the data from these AGN and the results of the analysis, in particular the characterization of the AGN continua and the warm absorption in AGN, have been discussed in detail by McKernan et al. (2005). In McKernan et al. (2004) we investigated this sample of AGN spectra for absorption due to local, highly ionized oxygen. Here we extend that study by searching for absorption in the vicinity of the Galaxy by metals other than oxygen. Our aim is to further the systematic study of the hot local gas and to begin constraining the temperatures and the relative metal abundances in the hot, local gas.

2 THE SAMPLE AND DATA ANALYSIS

Table 1 lists the AGN sample assembled by McKernan et al. (2005). Also listed in Table 1 are the AGN redshifts (from NED¹ using 21-cm H I radiation measurements where possible), the AGN Galactic latitude and longitude (also from NED), the Galactic column density and the total exposure times of the spectra. The sample, including selection criteria are discussed in detail in McKernan et al. (2005). The *Chandra* data were reprocessed and analysed according to the methods outlined in McKernan et al. (2005).

Here we extend the study of McKernan et al. (2004) by searching for evidence of absorption by metals less abundant than oxygen. Table 2 lists the relative solar abundances of the metals relevant for this study. Iron is the next most abundant metal after those listed in Table 2, but there is a forest of Fe L- and M-shell transitions in the soft X-ray band (see, e.g., Behar, Sako & Kahn 2001). There is therefore considerable ambiguity in Fe absorption-line identification due to blending. Furthermore, higher-order transitions of more abundant elements can also be misidentified as Fe transitions. Therefore, we limited our search to the strongest absorption transitions in the soft X-ray band in the most abundant highly stripped ions (not O VII and O VIII since we have studied these elsewhere); namely, N VII, Ne IX, Ne X, Mg XI, Mg XII, Si XIII and Si XIV, respectively. Table 3 lists the transitions that we investigated in this study, including their rest-frame wavelengths and oscillator strengths.

Once we measured the discrete absorption profiles, we used the extrapolated linear approximation to the curves of growth² to obtain

¹ <http://nedwww.ipac.caltech.edu/forms/byname.html>

² The linear part of the curves of growth implies that $N_{\text{ion}} = 1.13 \times 10^{17} \text{ EW} / f\lambda^2$, where N_{ion} is the ionic column density (cm^{-2}), EW is the equivalent width of the absorption feature (in mÅ), f is the oscillator strength of the transition and λ is in Å.

Table 1. The *Chandra* HETGS sample of type I AGN. Columns 2–4 give the Galactic coordinates and the redshift of the source (from NED). Redshift was deduced from observations of the 21-cm H I line where possible, since optical estimates of z may be confused by AGN outflow.

Source	Gal. long. (deg)	Gal. lat. (deg)	Redshift (z)	Gal. N_{H} (10^{20} cm^{-2}) ^a
Fairall 9	295.07	−57.83	0.04600	3.0
3C 120 ^b	190.37	−27.40	0.03301	12.30
NGC 3227	216.99	55.45	0.00386	2.15
NGC 3516	133.24	44.40	0.00884	3.05
NGC 3783	287.46	22.95	0.00973	8.50
NGC 4051	148.88	70.09	0.00242	1.31
Mrk 766	190.68	82.27	0.01293	1.80
NGC 4593	297.48	57.40	0.00831	1.97
MCG−6−30−15	313.29	27.68	0.00775	4.06
IC 4329a	317.50	30.92	0.01605	4.55
Mrk 279	115.04	46.86	0.03045	1.64
NGC 5548	31.96	70.50	0.01717	1.70
Mrk 509	35.97	−29.86	0.03440	4.44
NGC 7314	27.14	−59.74	0.00474	1.46
Akn 564	92.14	−25.34	0.02467	6.40

^aGalactic column density from Elvis, Wilkes & Lockman (1989), except for Mrk 509 (Murphy et al. 1996). The Galactic column density towards F9, NGC 3227, 3516, 3783, 5548, Mrk 766, NGC 7314 and Akn 564 was estimated from interpolations from the measurements of Stark et al. (1992).

^b3C 120 is also classified as a broad-line radio galaxy (NED).

Table 2. Relative solar element abundances relevant for this study. Values are taken from solar photospheric values of Anders & Grevesse (1989). Bahcall et al. (2005) suggest that the correct solar abundance of Ne is $[\text{Ne}/\text{H}] = 8.29 \pm 0.05$, values in parentheses use this value of the solar Ne abundance.

X	$\log(X/\text{O})_{\odot}$	$\log(X/\text{Ne})_{\odot}$	$\log(X/\text{Si})_{\odot}$
O	0.00	0.84(0.64)	1.38
Ne	−0.84(−0.64)	0.00	0.54(0.74)
N	−0.88	−0.04(−0.24)	0.50
Mg	−1.34	−0.50(−0.70)	0.04
Si	−1.38	−0.54(−0.74)	0.00

Table 3. Details of the discrete absorption transitions discussed in this study. f denotes the oscillator strength and λ denotes the wavelength (in Å) of the respective transitions (values from the Atomic Line List at <http://www.pa.uky.edu/~peter/atomic>).

Ion	Transition	f	$\lambda(\text{Å})$
N VII	Ly α	0.416	24.7810
Ne IX	(r)1s–2p	0.724	13.4473
Ne X	Ly α	0.415	12.1339
Mg XI	(r)1s–2p	0.742	9.1688
Mg XII	Ly α	0.415	8.4210
Si XIII	(r)1s–2p	0.757	6.6480
Si XIV	Ly α	0.414	6.1822

a lower limit on the ionic column density (N_{ion}), if a *lower limit* on the equivalent width (EW) of the absorption feature is available. Such a lower limit on N_{ion} is valid for any value of the velocity width (b) of the absorber. Where no lower limit on the EW exists,

Table 4. Results of spectral fitting for absorption due to hot Ne within $\pm 1200 \text{ km s}^{-1}$ from transition rest energies at $z = 0$. Of the four absorption features listed here, only one is likely to be mostly due to hot local gas (see the text for discussion). Columns 2 and 3 show the best-fitting EW for Ne IX (r) and Ne X Ly α , respectively, and (in parentheses) the improvement in the fit-statistic upon the addition of the inverted Gaussian model component to the continuum. Columns 4 and 5 show the ionic column densities of Ne IX and Ne X, respectively, as estimated from a curve-of-growth analysis (see the text for details). Column 6 shows the velocity centroid offset from $z = 0$ (LSR) of the Ne IX (r) and Ne X Ly α features, respectively. (log) Column densities are rounded to the nearest 0.05.

Sightline	EW(Ne IX (r)) (eV) (ΔC)	EW(Ne X Ly α) (eV) (ΔC)	$N_{\text{Ne IX}}$ (cm^{-2})	$N_{\text{Ne X}}$ (cm^{-2})	$v(\text{Ne IX})$ (km s^{-1})	$v(\text{Ne X})$ (km s^{-1})
NGC 4051	$2.64^{+0.79}_{-0.95}$ (17.6)	$1.14^{+0.54}_{-0.66}$ (7.2)	16.60 ± 0.15	$16.45^{+0.20}_{-0.40}$	$+420^{+520}_{-450}$	-175^{+205}_{-295}
MCG–6-30-15	$0.89^{+0.38}_{-0.50}$ (8.4)	$1.03^{+0.59}_{-0.48}$ (11.3)	$16.05^{+0.20}_{-0.25}$	$16.40^{+1/4}_{-0.35}$	-65^{+260}_{-165}	615^{+295}_{-235}

absorption is not significant (at 90 per cent confidence). However, in this case, for an assumed b value, we can use the *upper limit* on the EW to find an upper limit on N_{ion} . In such cases, we assumed a velocity width of $b \sim 100 \text{ km s}^{-1}$, since this is roughly the smallest width of a feature that the medium-energy grating (MEG) on *Chandra* can resolve, although it is considerably larger than the average value of $\langle b \rangle = 40 \pm 13 \text{ km s}^{-1}$ found by Sembach et al. (2003) in signatures of the local O VI absorption.

3 SPECTRAL FITTING

We used XSPEC version 11.2.0 for spectral fitting to the MEG spectra. All spectral fitting was carried out based on the best-fitting continuum models from McKernan et al. (2005). Spectral fitting was carried out in the 0.5–5 keV energy band, excluding the 2.0–2.5 keV region, which suffers from systematic effects as large as ~ 20 per cent in the effective area due to limitations in the calibration of the X-ray telescope.³ We analysed data binned at $\sim 0.02 \text{ \AA}$, which is approximately the MEG FWHM spectral resolution (0.023 \AA). This MEG spectral resolution corresponds to FWHM velocities of ~ 280 and 560 km s^{-1} at observed energies of 0.5 and 1.0 keV, respectively. We used the C-statistic (Cash 1976) to find best-fitting model parameters and quote 90 per cent confidence, one-parameter errors.

We proceeded to fit the MEG spectra for the discrete absorption transitions in Table 3 by adding an inverted Gaussian model component to the best-fitting continuum models detailed in McKernan et al. (2005). The width of the inverted Gaussian was chosen to be $> 100 \text{ km s}^{-1}$, which is approximately the lower limit of the instrumental velocity resolution. We fixed the redshift of the Gaussian components at $z = 0$ and allowed the rest energy of the component to vary by $\pm 1200 \text{ km s}^{-1}$ from the rest-frame energies of the transitions listed in Table 3. The allowed velocity range is identical to that used by Sembach et al. (2003) and McKernan et al. (2004) in searches for highly ionized oxygen absorption in the vicinity of the Milky Way.

4 RESULTS

Of the 15 AGN sightlines in our sample, only the sightlines to NGC 4051 and MCG–6-30-15 exhibit absorption features within $\pm 1200 \text{ km s}^{-1}$ of their rest-frame energy at $z = 0$ at ≥ 99 per cent confidence ($\Delta C \geq 11.3$ for three additional parameters). The sightlines to F9, NGC 4593, 3227 and MCG–6-30-15 exhibit absorption features within $\pm 1200 \text{ km s}^{-1}$ of their rest-frame energy at $z = 0$ at ≥ 90 per cent but ≤ 99 per cent confidence. Of the metals we searched

Table 5. As for Table 4, except for Mg XII Ly α and Si XIV Ly α along the sightline to MCG–6-30-15. These features are kinematically consistent with the Ne X Ly α feature along this sightline in Table 4 above. Therefore, these absorption features are most likely to be due to a hot absorbing outflow from MCG–6-30-15 at $\sim -1710 \text{ km s}^{-1}$ (see the text).

Transition	EW (eV) (ΔC)	N (cm^{-2})	Vel. (km s^{-1})
Mg XII Ly α	$1.56^{+1.10}_{-0.98}$ (8.2)	$16.55^{+0.20}_{-0.40}$	$+530^{+450}_{-550}$
Si XIV Ly α	$2.96^{+0.98}_{-1.01}$ (23.1)	$16.60^{+0.15}_{-0.20}$	$+615^{+255}_{-285}$

for, only Ne, Mg and Si absorption signatures were detected at > 90 per cent confidence.

Tables 4 shows the best-fitting model parameters for the strongest detections of Ne IX (r) and Ne X Ly α absorption features. The strongest absorption signatures lie along the sightlines to NGC 4051 and MCG–6-30-15, respectively, where at least one of the Ne absorption features has been detected at ≥ 99 per cent confidence. Table 5 similarly details the best-fitting model parameters from a detection of Si XIV Ly α at $> 3\sigma$ significance and a detection of Mg XII Ly α at > 90 per cent confidence along the sightline to MCG–6-30-15. Listed in Tables 4 and 5 are the equivalent widths of the absorption features and (in parentheses) the improvement in the C-statistic upon addition of the inverted Gaussian model component to the continuum. Also listed in Tables 4 and 5 are the velocity offsets from $z = 0$ of the respective Gaussian centroids and limits on the respective ionic column densities as estimated from a curve-of-growth analysis as outlined above in Section 2.

Although the features listed in Tables 4 and 5 are statistically significant, the kinematics of most of these features could be consistent with originating in an AGN outflow. The absorption features detected towards NGC 4051 for example, are barely kinematically consistent with an origin in gas at $z = 0$, or indeed with an origin in the same gas (within 90 per cent errors, see Table 4). Nevertheless, at $c z = 725 \text{ km s}^{-1}$, NGC 4051 is very near and with a *Chandra* gratings energy resolution of FWHM $\sim 500 \text{ km s}^{-1}$ at the energy of the Ne IX (r) transition (0.922 keV), it is kinematically difficult to distinguish X-ray absorption intrinsic to the NGC 4051 outflow from X-ray absorption due to hot local gas. Some or most of this hot gas may be associated with the warm absorbing outflow in this AGN.

Along the MCG–6-30-15 sightline, only the Ne IX (r) absorption feature is kinematically consistent with $z = 0$ absorption. The Ne X Ly α absorption feature in Table 4 (at $+615^{+295}_{-235} \text{ km s}^{-1}$), coincides kinematically with the Si XIV Ly α and Mg XII Ly α absorption features in Table 5 (at $\sim +615$ and $\sim +530 \text{ km s}^{-1}$), but these features are not kinematically consistent with an origin in hot local

³ <http://asc.harvard.edu/udocs/docs/POG/MPOG/node13.html>

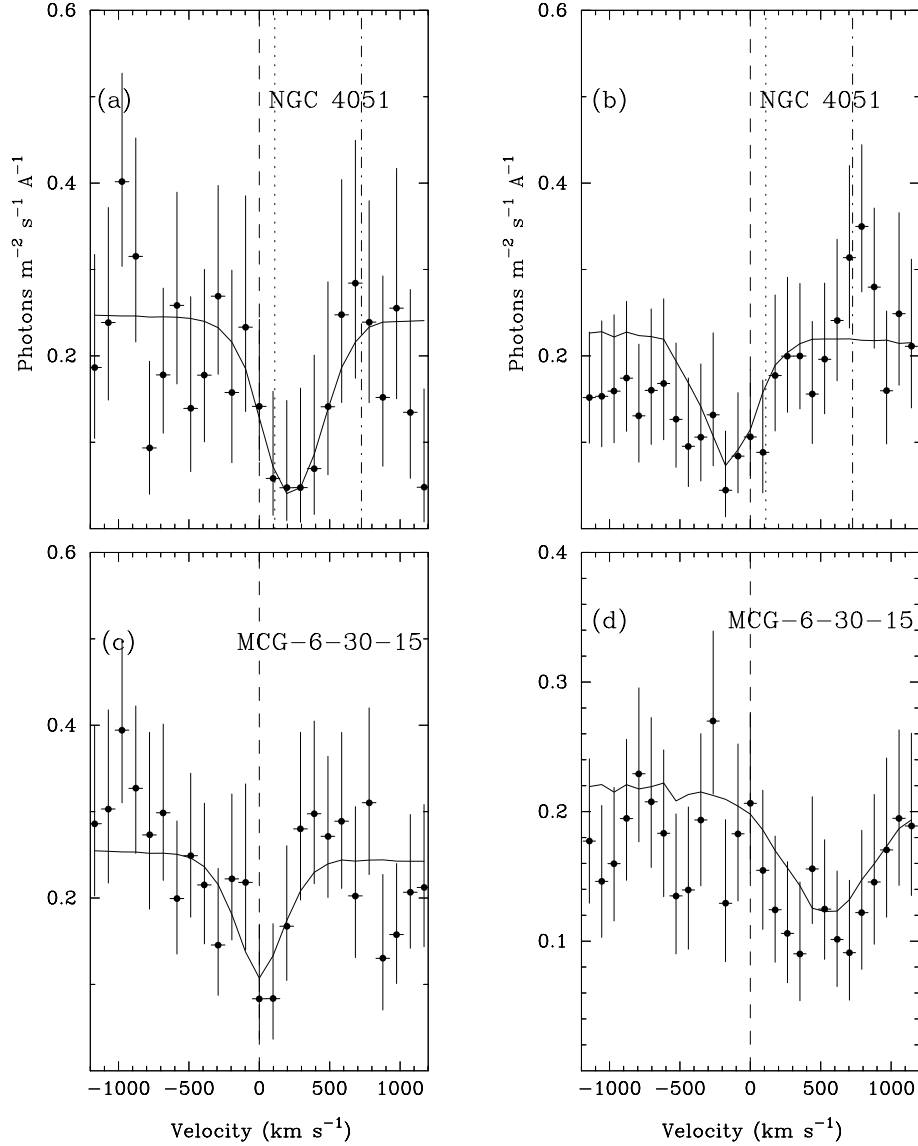


Figure 1. Velocity profiles from combined ± 1 order *Chandra* MEG data from the AGN in Table 4, centred on the LSR Ne IX (r) transition energy (0.9220 keV) in the left-hand panels and on the Ne X Ly α transition energy (1.0218 keV) in the right-hand panels (dashed lines). A positive velocity indicates a redshift relative to these energies. The velocity spectra data have been uniformly binned at 0.3 eV, which is approximately the limit of the MEG resolution [0.3 eV is the FWHM resolution at ~ 0.4 keV or about one-fifth the FWHM at the Ne IX (r) transition energy]. Vertical dotted lines in (a) and (b) indicate the weighted mean offset velocity $cz = +110 \pm 115$ km s $^{-1}$ of absorption due to O VII and O VIII (from McKernan et al. 2004). Vertical dash-dot lines indicate the rest-frame of NGC 4051 ($cz = 726$ km s $^{-1}$). The rest frame of MCG-6-30-15 ($cz = 2325$ km s $^{-1}$) lies outside the ± 1200 km s $^{-1}$ range of these panels. Superposed is the best-fitting inverted Gaussian absorption-line model (from Table 4) and continuum (horizontal solid line). Of the four profiles shown here, only the Ne IX (r) feature towards MCG-6-30-15 is likely to be entirely due to hot, local gas (see the text). The features towards NGC 4051 are most likely to be due in large part to a warm absorbing outflow from this AGN.

gas at $z = 0$. Thus, we conclude that the Ne X Ly α , Si XIV Ly α and Mg XII Ly α features along the sightline to MCG-6-30-15 originate in a warm absorber outflowing from the AGN at -1710 km s $^{-1}$ rather than hot local gas (see also McKernan et al. 2005). Therefore, in order to study the hot *local* Ne X Ly α along the sightline to MCG-6-30-15, we searched for upper limits on absorption due to Ne X Ly α by adding a narrow inverted Gaussian to the spectrum at -65 km s $^{-1}$ from $z = 0$ rest-frame energy [to compare with the corresponding Ne IX (r) absorption]. We obtained upper limits on absorption due to Mg XII Ly α and Si XIV Ly α similarly by adding a narrow inverted Gaussian at the $z = 0$ rest-frame energy of the transition. Likewise, for NGC 4051, we obtained upper

limits on absorption due to Ne IX and Ne X by adding narrow inverted Gaussians at the rest-frame energy of the respective absorption transitions at $z = 0$.

Fig. 1 is a multipanel plot showing velocity profiles of the Ne IX (r) and Ne X Ly α absorption features along the sightlines to NGC 4051 and MCG-6-30-15. The profiles are centred on the Ne IX (r) transition energy (0.9220 keV) and the Ne X Ly α transition energy (1.0218 keV) in the local standard of rest (LSR), respectively (both energies are denoted by vertical dashed lines at 0 km s $^{-1}$). The vertical dotted line in Fig. 1(a,b) at $+110$ km s $^{-1}$ denotes the weighted mean offset velocity of the O VII and O VIII absorption along this sightline detected by McKernan et al. (2004). The vertical dash-dot

line in Figs 1(a) and (b) at $+725 \text{ km s}^{-1}$ denotes the recessional velocity (c_z) of NGC 4051. Superposed on the data is the best-fitting inverted Gaussian absorption-line model (from Table 4) and continuum (horizontal solid line).

Of the less significant absorption features detected (at ≥ 90 per cent confidence but < 99 per cent confidence), those along the sightlines towards F9 and NGC 4593 are kinematically coincident with their rest energies at $z = 0$ and are therefore likely to correspond to hot local gas. A Si xiv Ly α feature detected at an offset velocity of $-525_{-600}^{+450} \text{ km s}^{-1}$ along the sightline towards NGC 3227 is more likely to correspond kinematically to an outflow at $\sim 1700 \text{ km s}^{-1}$ from the AGN ($c_z = 1160 \text{ km s}^{-1}$) than absorption due to hot, local gas. We obtained upper limits on absorption due to Si xiv along this sightline by fitting a narrow inverted Gaussian to the continuum at the rest energy of Si xiv Ly α at $z = 0$.

4.1 Local, hot gas versus AGN outflow?

NGC 4051 and MCG–6-30-15 are two of the closest AGN in our sample, at recessional velocities of $c_z = 726$ and 2325 km s^{-1} , respectively. Since the spectra of Type I AGN typically exhibit hot gas outflowing at several hundred km s^{-1} , the proximity of these two AGN raises the important issue of confusion between absorption due to hot gas at $z = 0$ and that due to a warm absorber (see also the discussion in McKernan et al. 2004). The proximity of NGC 4051 and MCG–6-30-15 (and NGC 3227) and the limited gratings spectral resolution makes it difficult to distinguish X-ray absorption features along these sightlines due to hot local gas from those due to warm absorbing outflows. On the other hand, the more distant the AGN, the more likely it is that absorption signatures at offset velocities very close to their $z = 0$ rest-frame energy are due to hot, local gas. The relation in fig. 3 of McKernan et al. (2004) shows this effect quite dramatically. Thus, outflows previously thought to be associated with more distant AGN, e.g. PG 1211+143 (Pounds et al. 2003) and PDS 456 (Reeves, O’Brien & Ward 2003) are kinematically much more likely to correspond to hot, local gas. We note that the surprisingly high Fe column densities towards both of these AGN might be accounted for by the intersection of both of these

sightlines with the limb of the local Northern Polar Spur (NPS) structure. A third sightline through the NPS, towards MCG–6-30-15 also exhibits strong absorption due to a large column of highly ionized Fe that is kinematically consistent with a local origin (Young et al. 2005). The NPS is a local feature believed to correspond to the superposition of several supernovae and is clearly seen in X-ray emission maps (see, e.g., Snowden et al. 1997) and in maps of polarization towards nearby stars (Mathewson & Ford 1970; Axon & Ellis 1976; Heiles & Jenkins 1976). An alternative hypothesis is that the NPS may actually be a much larger feature subtended at the Galactic centre (Sofue 2000; Bland-Hawthorn & Cohen 2003), although we shall not consider this hypothesis further here. If the progenitor supernovae of the NPS were rich in pure Fe, this could account for the anomalous column of Fe along these sightlines. We intend to investigate this possibility in future work.

4.2 Column densities of hot local metals

Table 6 lists the limits on the ionic column densities for all the ions from spectral fitting. Most of the results in Table 6 are upper limits, indicating that discrete absorption features due to local gas are not detected at > 90 per cent confidence in most cases. None of the sightlines exhibited absorption due to local N at > 90 per cent confidence. The spectra of three AGN, namely NGC 3227, 3516 and 7314, were too heavily absorbed at $\leq 0.8 \text{ keV}$ to even obtain meaningful limits on N VII absorption. We found that assuming different values of the velocity width (e.g. $b \sim 50$ or $\sim 200 \text{ km s}^{-1}$), led to small changes in estimates of N_{ion} in Table 6, $\log(\Delta N_{\text{ion}}) < 0.2$ for $b = 50 \text{ km s}^{-1}$ and $\log(\Delta N_{\text{ion}}) < 0.1$ for $b = 200 \text{ km s}^{-1}$, respectively, using the linear part of the curves of growth.

Sembach et al. (2003) and McKernan et al. (2004) associate local, highly ionized O absorption with known local structures such as the Magellanic Stream (MS), Complex C and Extreme Positive North (EPN), as well as a diffuse local group (LG) and (potentially) the warm/hot IGM. Several of the sightlines in Table 6 can be identified with these structures: one (F9) with the MS, three (NGC 4593, 4051 and 3227) are identified with EPN and one (MCG–6-30-15) which we associate with the NPS. In the southern Galactic hemisphere, the

Table 6. Results of spectral fitting for hot gas at $z = 0$ as discussed in the text. Columns 2–8 show the logarithm of the ionic column densities of N VII, Ne IX, Ne X, Mg XI, Mg XII, Si XIII and Si XIV, respectively, as estimated from a curve-of-growth analysis as described in the text. (log) Column densities are rounded to the nearest 0.05. Lower limits on ionic column densities are valid for all values of b . Upper limits are valid for an assumed velocity width of 100 km s^{-1} (unless specified otherwise) which is approximately the lower bound on the instrumental resolution. A choice of $b = 100 \text{ km s}^{-1}$ is larger than the values inferred by S03 for local O VI absorption features.

Sightline	(log) $N_{\text{N VII}}$ (cm^{-2})	$N_{\text{Ne IX}}$ (cm^{-2})	$N_{\text{Ne X}}$ (cm^{-2})	$N_{\text{Mg XI}}$ (cm^{-2})	$N_{\text{Mg XII}}$ (cm^{-2})	$N_{\text{Si XIII}}$ (cm^{-2})	$N_{\text{Si XIV}}$ (cm^{-2})
F9	<15.30	<17.00	$16.35_{-0.35}^{+1/4}$	<16.15	<16.60	<17.30	<16.10
3C 120	<18.60	<16.90	<15.85	<15.70	<16.75	<16.65	<16.20
NGC 3227	^a	<16.40	<16.70	<18.95	<16.90	<17.75	<17.10
NGC 3516	^a	<16.70	<16.95	<16.15	<16.30	<17.35	<16.70
NGC 3783	<15.80	<15.80	<14.95	<15.75	< 15.20	<14.75	<14.90
NGC 4051	<16.70	<15.90	<16.80	<16.65	<16.60	<17.75	<16.70
Mrk 766	<16.95	<15.85	<16.10	<16.40	<16.35	<17.30	<16.25
NGC 4593	<16.65	$16.05_{-0.80}^{+1/4}$	<16.10	<16.20	<16.15	<16.35	<16.45
MCG–6-30-15	<16.65	$16.05_{-0.25}^{+0.20}$	<16.25	<18.15	<16.55	<15.95	<16.50
IC 4329A	<17.70	<16.50	<15.95	<15.50	<16.35	<15.90	<16.25
Mrk 279	<16.10	<16.50	<16.45	<16.80	<16.50	<16.05	<16.45
NGC 5548	<16.40	<16.10	<16.80	<16.40	<16.35	<16.20	<16.35
Mrk 509	<16.45	<16.20	<15.80	<16.10	<16.10	<16.05	<15.80
NGC 7314	^a	<17.05	<16.80	<15.90	<16.50	<17.55	<16.45
Akn 564	<16.20	<15.85	<15.85	<16.20	<16.35	<16.75	<16.20

^a The soft X-ray spectrum is too absorbed to obtain limits.

sightline to Akn 564 passes through the Magellanic Stream extension (MSe), but this may also be LG (Sembach et al. 2003).

Sembach et al. (2003) conclude that most of the high-velocity ($v \sim 100\text{--}400 \text{ km s}^{-1}$) O VI gas in the vicinity of the galaxy is created by collisional ionization. Furthermore, gas in the low-redshift IGM is far more likely to be collisionally ionized than photoionized (Heckman et al. 2002). Therefore, if we assume that the hot gas in the vicinity of the Galaxy is in collisional ionization equilibrium (CIE), and that the absorption signatures discussed here and in McKernan et al. (2004) are due to the same gas, it is possible to establish temperature constraints on the gas, whether it is local to our Galaxy or low-redshift WHIGM. Sutherland & Dopita (1993) calculate $N_{\text{Ne IX}}/N_{\text{Ne X}}$ and $N_{\text{Si XIII}}/N_{\text{Si XIV}}$ for gas in CIE, so where there are statistically significant lower limits on an ionic column along a given sightline, we can constrain the temperature of local gas along that sightline with some confidence. However, from searching for seven absorption transitions along each of 15 different sightlines through the hot, local gas, there are only three *lower* limits on ionic column densities. The corresponding temperature limits (assuming CIE) using the $N_{\text{Ne IX}}/N_{\text{Ne X}}$ ratio are: $T < 10^{6.75} \text{ K}$ towards MCG-6-30-15, $T < 10^{6.70} \text{ K}$ towards NGC 4593 and $T > 10^{6.35} \text{ K}$ towards F9. The sightline to F9 provides a *lower* limit on the temperature because we detect Ne X Ly α and not Ne IX (λ 7774) (McKernan et al. 2004).

5 COMPARISON WITH SIGNATURES OF OXYGEN ABSORPTION

McKernan et al. (2004) showed that seven of the 15 sightlines in our sample exhibit discrete absorption features due to local O VII and O VIII. Sembach et al. (2003) found local O VI (λ 1031.926) absorption along 59 of 102 sightlines towards UV bright AGN/quasistellar objects at high Galactic latitudes ($|b| \geq 30^\circ$). Several of the 59 sightlines coincide with sightlines in our sample (F9, NGC 5448, Mrk 509, Akn 564), of which three (F9, Mrk 509, Akn 564) show significant O VI absorption. In Fig. 2, we show the sightlines to the 15 AGN in our sample in the Hammer-Aitoff projection. Crosses indicate non-detection of *any* highly ionized local gas (Ne, Mg, Si and O) along the sightline. Triangles indicate detection (at

>90 per cent confidence) of highly ionized local gas (Ne or Si) with no corresponding highly ionized O. Diamonds indicate the presence of local, highly ionized O along the sightline, but non-detection of local, highly ionized Ne, Mg and Si. Filled-in circles indicate sightlines along which highly ionized Ne or Si has been detected (at >90 per cent confidence) *and* which show absorption due to local, highly ionized O.

Of the three sightlines which exhibit absorption by local, highly ionized Ne at >90 per cent confidence (listed in Table 6), two sightlines (F9 and NGC 4593) also exhibit absorption by O VII and/or O VIII at >90 per cent confidence (McKernan et al. 2004). The sightline towards F9 also exhibits O VI absorption (Sembach et al. 2003). The sightlines to MCG-6-30-15 does not exhibit absorption due to highly ionized oxygen. In McKernan et al. (2004) we constrained the temperature in local gas from limits on $N_{\text{O VIII, VII, VI}}$ and an assumption of CIE. Towards F9, we found $10^{5.75} < T < 10^{6.35} \text{ K}$. This is marginally inconsistent with our estimate of $T > 10^{6.35} \text{ K}$ using $N(\text{Ne IX, Ne X})$ in Section 4 above. However, the condition that $T < 10^{6.35} \text{ K}$ along this sightline is derived assuming a b parameter of precisely 100 km s^{-1} using $N_{\text{O VIII}}$ in a curve-of-growth analysis. A choice of a slightly larger b parameter (which would be allowed by the data) would yield a temperature upper limits compatible with that derived using $N(\text{Ne IX, Ne X})$. The combined results using $N(\text{O VI, O VII, O VIII, Ne IX and Ne X})$ along the sightline to F9, suggests that the temperature in the local hot gas in the MS is close to $T \sim 10^{6.35} \text{ K}$ and that there is some velocity broadening of the hot gas along this sightline. The temperature of the gas along the sightlines to NGC 5448 and Akn 564 was also constrained by McKernan et al. (2004) to be $T > 10^{6.2}$ and $< 10^{6.1} \text{ K}$, respectively. However, the absence of significant absorption along the sightlines to NGC 5548 and Akn 564 in this study (see Table 6), means that we cannot provide additional constraints on the temperature of gas along these sightlines.

6 POSSIBLE CONSTRAINTS ON METALLICITIES IN HOT LOCAL GAS

The temperature ranges derived from the ratios of column densities in Section 4 above and by Sembach et al. (2003) and McKernan

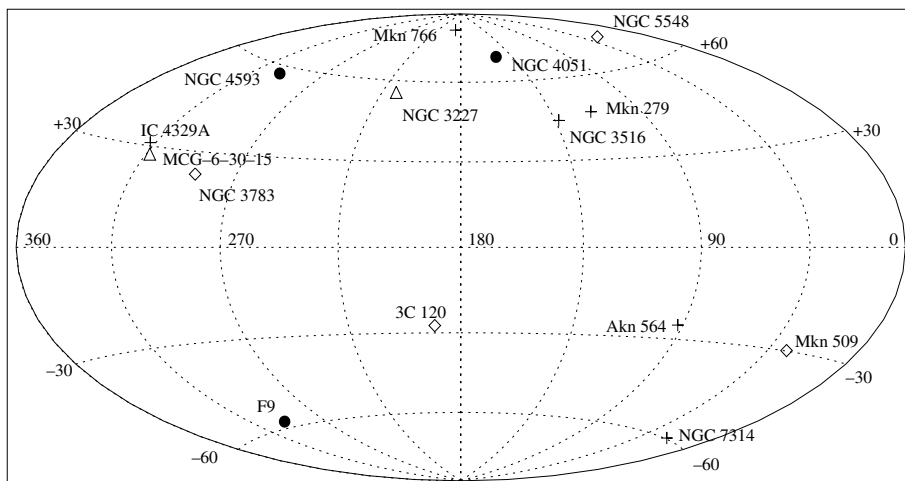


Figure 2. All-sky Hammer-Aitoff projection of the sightlines to the 15 AGN in this study. In this projection, the Galactic anticentre is at the centre of the figure and Galactic longitude increases to the left. Crosses indicate non-detection of local, highly ionized Ne, Mg, Si or O along the sightline (measurements of O from McKernan et al. 2004). Diamonds indicate non-detection of local, highly ionized Ne or Si, but detection of highly ionized O along the sightline. Triangles indicate detection of local, highly ionized Ne or Si along the sightlines at >90 per cent confidence, but no corresponding absorption due to local, highly ionized O. Filled-in circles denote detection of local, highly ionized Ne or Si along the sightlines at >90 per cent confidence *plus* corresponding local, highly ionized O absorption.

et al. (2004) suggest that we can assume that most of the O, Ne, Mg and Si in the hot gas in the vicinity of the Galaxy is in H-like and He-like ions. If we assume that the gas is in CIE, then for a range of temperatures, such as those discussed here, the fraction in H-like or He-like ions is much larger than in other ionic states (Sutherland & Dopita 1993, e.g. in the case of oxygen ions, $O\text{ VIII}/O\text{ IX} \gg 1$, $O\text{ VII}/O\text{ VI} \gg 1$). Thus, in a simple approximation, the largest upper (or lower) limit on the column density of the He-like or H-like ions of a particular element is approximately the upper (lower) bound on the amount of the element present.

Therefore, given a lower limit to the column density $N(X)$ of an element X , using this simple approximation, we can use upper limits on the column density $N(Y)$ of element Y to obtain a lower limit on $N(X)/N(Y)$ along a sightline. Limits on relative metal abundances in the hot local gas, allow us to compare the results with solar relative abundances (see Table 1) and thereby establish limits on the composition of the hot gas. The relative depletion or enrichment of certain metals can provide clues to the environment, formation and evolution of the hot gas in local structures and the hot IGM. Note that it is not possible to obtain reliable upper limits on the ratio $N(X)/N(Y)$, since an upper limit on $N(X)$ is potentially much more inaccurate than a lower limit (a firm lower bound on the column), due to the possibility of additional columns of more or less ionized gas than those considered here.

Tables 7 and 8 list constraints on the metal abundances relative to O and Ne, respectively, in the hot gas in the vicinity of our Galaxy. Clearly, the lower limits on the relative abundances in the local, hot gas are in general too small to be interesting, with a few exceptions. In Table 7, the lower limit on $[O/N]$ along the sightline to F9 is close to the solar value, while the other ratios are one or two orders of magnitude lower, which may suggest a relative underabundance of N in the MS. Also in Table 7, the lower limit on $[O/Si]$ along the sightline to NGC 3783 is close to the solar ratio, while the other

Table 7. The (log) abundances of elements relative to oxygen in the hot gas in the vicinity of the Galaxy, assuming CIE. Values in parentheses correspond to a solar Ne abundance from Bahcall et al. (2005).

Sightline	[O/Ne]	[O/N]	[O/Mg]	[O/Si]
☉	0.84(0.64)	0.90	1.29	1.38
F9	>−0.90	>0.80	>−0.50	>−1.20
3C 120	>−1.22	>−2.86	>−1.03	>−0.47
NGC 3783	>0.04	>0.06	>0.08	>0.95
NGC 4051	>−0.35	>−0.24	>−0.22	>−1.30
NGC 5548	>−0.87	>−0.46	>−0.49	>−0.42
Mrk 509	>−0.93	>−1.16	>−0.85	>−0.77

Table 8. The (log) abundance of Ne relative to O, N, Mg and Si in the hot gas in the vicinity of the Galaxy. We assumed CIE in calculating these ratios. Values in parentheses correspond to a solar Ne abundance from Bahcall et al. (2005).

Sightline	[Ne/O]	[Ne/N]	[Ne/Mg]	[Ne/Si]
☉	−0.84(−0.64)	0.04(0.24)	0.50(0.70)	0.54(0.74)
F9	^a	>0.70	>−0.60	>−1.30
NGC 4593	>−1.99	>−1.41	>−0.96	>−1.19
MCG−6-30-15	>−0.85	>−0.60	>−0.15	>−0.60

^aThere is no meaningful upper limit on $N(O)$ for the sightline to F9, since $\log N(O\text{ VII}) > 16.1$ (possible saturation) and $\log N(O\text{ VIII}) < 16.6$ (McKernan et al. 2004).

ratios are significantly lower, which may be hinting at a relative underabundance of Si along this sightline. In Table 8, $[Ne/N]$ along the sightline to F9 exceeds the solar value by ~ 3.9 , and $[Ne/Si]$ along the sightline to MCG−6-30-15 is roughly solar. The other Ne ratios are one or two orders of magnitude below their solar values. This again suggests an underabundance of N in the hot gas in the MS.

7 CONCLUSIONS

Half of the baryonic matter in the local universe seems to be missing. The search for the hottest component of the missing matter has only been possible with the latest generation of high spectral resolution X-ray telescopes. Hot gas in the vicinity of the Galaxy may be due to local WHIGM or it may reside either in a hot Galactic halo or locally in a thick disc and has only recently begun to be studied in the X-ray band. We assembled a small sample of type I AGN observed with the high-resolution X-ray gratings on board *Chandra* and we have applied a uniform analysis to detect soft X-ray absorption by hot gas in the vicinity of our Galaxy. This study is an extension of our previous study of $O\text{ VII}$ and $O\text{ VIII}$ absorption by hot local gas (McKernan et al. 2004).

Three of the 15 sightlines in our sample (towards F9, NGC 4593 and MCG−6-30-15, respectively) exhibit Ne IX (r) or Ne X Ly α absorption due to hot, local gas at ≥ 90 per cent confidence. We identify these absorption features with the hot phase of local structures. Such local structures are either in the disc of the Galaxy (e.g. the Local Bubble or superbubbles such as the NPS) or lie above the disc in high-velocity clouds (HVCs) or other structures, such as a Galactic halo. Hot gas in a thick disc is expected to have a low offset velocity from $z = 0$ (typically $\leq 100\text{ km s}^{-1}$) and hot gas above the disc in HVCs or in a Galactic halo is expected to have a higher offset velocity from $z = 0$ (typically $100\text{--}400\text{ km s}^{-1}$). The sightlines to the AGN in our sample lie well away from the Galactic plane ($b \geq 30^\circ$) and *Chandra* does not possess the velocity resolution to distinguish between kinematic signatures of a thick disc or Galactic halo. Therefore, we cannot tell whether absorption is local to the disc, or further out in a halo, where there are no known local structures along a sightline. Absorption studies in the UV band with *FUSE* indicate that there is a thick Galactic disc of $O\text{ VI}$, with a scaleheight of $\sim 2.3\text{ kpc}$, as well as a patchy overdensity of $O\text{ VI}$ in the northern Galactic hemisphere from $b \sim 45^\circ$ to 90° due to the Local Bubble and superbubbles (including the NPS) (Savage et al. 2003). X-ray spectral studies of Galactic X-ray binaries confirm that there is a hot, thick disc with a scaleheight of $\sim 1\text{--}2\text{ kpc}$ associated with our Galaxy (see, e.g., Futamoto et al. 2004; Yao & Wang 2005). The column densities inferred from Futamoto et al. (2004) and Yao & Wang (2005) are consistent with the limits inferred here, so it may be that most or all of the hot gas locally is associated with a Galactic ‘thick disc’ of hot gas, with enrichment along particular sightlines in the northern Galactic hemisphere due to local superbubbles such as the NPS.

There can be considerable ambiguity in distinguishing local hot absorbing gas and hot absorbing outflows from AGN, especially with the limited spectral resolution of the *Chandra* gratings. This is particularly true of some of the AGN in the present study. Two sightlines in our study (towards MCG−6-30-15 and NGC 4051, respectively) exhibit absorption features within $\pm 1200\text{ km s}^{-1}$ of their rest energies at $z = 0$ at confidence levels of >99 per cent. However, the kinematics of the absorption signatures suggest that these features are most likely to be due to absorption in hot gas outflowing from the respective background AGN. Nevertheless, the more

distant the AGN, the more likely that absorption signatures in the AGN spectrum which kinematically coincide with the AGN recession velocity are due to hot, local gas. This is demonstrated by the relation in fig. 3 of McKernan et al. (2004). Two of the AGN in fig. 3 of McKernan et al. (2004), namely PG 1211+143 and PDS 456, also exhibit absorption due to a very large local column of Fe, which is surprising. We point out that absorption by the local NPS bubble, if Fe-enriched, could account for the very large column density of Fe along the sightline to these AGN, and towards MCG-6-30-15 as well. Thus, hot gas in the disc of the Galaxy may account for much of the $z = 0$ absorption in the soft X-ray spectra of several AGN.

We assumed collisionally ionized equilibrium to use limits on ionic column densities to derive limits on the temperatures in the hot, local gas. We find that in the southern Galactic hemisphere, the sightline to F9 through the MS yields $T > 10^{6.35}$ K, which is marginally consistent with our temperature limits from $N(\text{O VII})/N(\text{O VIII})$ (McKernan et al. 2004). Likewise, in the northern Galactic hemisphere we find temperature limits of $T < 10^{6.75}$ K towards MCG-6-30-15 and $T < 10^{6.70}$ K towards NGC 4593. For a range of temperatures, such as those discussed here, derived limits on the H- and He-like ion column densities allow us to establish constraints on the relative abundances of N, Ne, Mg and Si [as well as O from McKernan et al. (2004)] along the sightlines in our sample. In general, we found lower limits on the relative abundances of the metals that are one or two orders of magnitude below the corresponding solar values (see Tables 7 and 8). However, we do find evidence for a relative *underabundance* of N in the hot gas in the MS along the sightline towards F9.

The question of whether the hot gas detected in the vicinity of the Galaxy is in part (or at all) associated with the missing matter remains as yet unanswered. The environment of the Galaxy is complex, consisting of satellite galaxies (Magellanic Clouds), tidal trails (the Magellanic Stream), infalling HVCs and outflows from supernovae in the Galaxy. Standard theories of structure formation in the universe suggest that our Local Group (our Galaxy and M31) should have formed from a low-density filament of gas, the heated remnants of which should persist today. The local filament should be metal-enriched by outflows from structures that formed within it. However, the upper limits on column densities that we derive here and in McKernan et al. (2004) seem to be consistent with estimates of column densities from studies of Galactic haloes in edge-on normal spiral galaxies (Strickland et al. 2004). Thus, our first systematic (but hardly comprehensive) look at the hot, X-ray absorbing component of gas in the vicinity of our Galaxy suggests that our Galaxy is embedded in a hot halo or hot thick disc.

ACKNOWLEDGMENTS

We gratefully acknowledge support from NSF grant AST0205990 (BM) and NASA grant AR4-5009X issued by CXC operated by SAO under NASA contract NAS8-39073 (TY). We made use of the HEASARC on-line data archive services, supported by NASA/GSFC and also of the NASA/IPAC Extragalactic Data base (NED), operated by the Jet Propulsion Laboratory, CalTech, under contract with NASA. Thanks to the *Chandra* instrument and operations teams for making the observations possible. Thanks to M. Coleman Miller, David Strickland and Andy Fabian for useful

discussions and thanks to Ken Sembach for bringing to our attention the uncertainty in the solar Ne abundance. Thanks to the anonymous referee for their comments which helped to improve this paper.

REFERENCES

- Anders E., Grevesse N., 1989, *Geochim. Cosmochim. Acta*, 53, 197
 Axon D. J., Ellis R. S., 1976, *MNRAS*, 177, 499
 Bahcall J. N., Basu S., Serenelli A. M., 2005, *ApJ*, in press (astro-ph/0502563)
 Behar E., Sako M., Kahn S. M., 2001, *ApJ*, 570, 165
 Bland-Hawthorn J., Cohen M., 2003, *ApJ*, 582, 246
 Cagnoni I., 2002, preprint (astro-ph/0212070)
 Cash W., 1976, *A&AS*, 52, 307
 Cen R., Ostriker J. P., 1999, *ApJ*, 514, 1
 Collins J. A., Shull J. M., Giroux M. L., 2004, *ApJ*, 605, 216
 Davé R. et al., 2001, *ApJ*, 552, 473
 Elvis M., Wilkes B. J., Lockman F. J., 1989, *AJ*, 97, 777
 Fang T., Marshall H. L., Lee J. C., Davis D. S., Canizares C. R., 2002, *ApJ*, 572, L127
 Fang T., Sembach K. R., Canizares C. R., 2003, *ApJ*, 586, L49
 Futamoto K., Mitsuda K., Takei Y., Fujimoto R., Yamasaki N. Y., 2004, *ApJ*, 605, 793
 Heckman T. M., Norman C., Strickland D. K., Sembach K. R., 2002, *ApJ*, 577, 691
 Heiles C., Jenkins E. B., 1976, *A&A*, 46, 333
 Hellsten U., Gnedin N. Y., Miralde-Escudé J. M., 1998, *ApJ*, 509, 56
 Kang H., Ryu D., Cen R., Song D., 2005, *ApJ*, 620, 21
 McKernan B., Yaqoob T., George I. M., Turner T. J., 2003a, *ApJ*, 593, 142
 McKernan B., Yaqoob T., Mushotzky R., George I. M., Turner T. J., 2003b, *ApJ*, 598, L83
 McKernan B., Yaqoob T., Reynolds C. S., 2004, *ApJ*, 617, 232
 McKernan B., Yaqoob T., Reynolds C. S. 2005, *MNRAS*, submitted
 Markert T. H., Canizares C. R., Dewey D., McGuirk M., Pak C., Shattenburg M. L., 1995, *Proc. SPIE*, 2280, 168
 Mathewson D. S., Ford V. L., 1970, *MNRAS*, 74, 139
 Murphy E. M., Lockman F. J., Laor A., Elvis M., 1996, *ApJS*, 105, 369
 Nicastro F. et al., 2002, *ApJ*, 573, 157
 Nicastro F. et al., 2005, *Nat*, 433, 495
 Perna R., Loeb A., 1998, *ApJ*, 503, L135
 Pounds K. A., Reeves J. N., King A. R., Page K. L., O'Brien P. T., Turner M. J. L., 2003, *MNRAS*, 345, 705
 Rasmussen A., Kahn S. M., Paerels F., 2002, *The IGM/Galaxy Connection – the Distribution of Baryons at $z = 0$* . Kluwer, Dordrecht (astro-ph/0301183)
 Ravasio M., Tagliaferri G., Pollock A. M. T., Ghisellini G., Tavecchio F., 2005, *A&A*, in press (astro-ph/0502567)
 Reeves J. N., O'Brien P. T., Ward M. J., 2003, *ApJ*, 593, L65
 Savage B. D. et al., 2003, *ApJS*, 146, 125
 Sembach K. R. et al., 2003, *ApJS*, 146, 165
 Snowden S. L. et al., 1997, *ApJ*, 485, 125
 Sofue Y., 2000, *ApJ*, 540, 224
 Stark A. A. et al., 1992, *ApJS*, 79, 77
 Strickland D. K., Heckman T. M., Colbert E. J. M., Hoopes C. G., Weaver K. A., 2004, *ApJS*, 151, 193
 Sutherland R. S., Dopita M. A., 1993, *ApJS*, 88, 253
 Tripp T. M., Savage B. D., Jenkins E. B., 2000, *ApJ*, 534, L1
 Yao Y., Wang Q. D., 2005, *ApJ*, 624, 751
 Young A. J., Lee J. C., Fabian A. C., Reynolds C. S., Gibson R. R., Canizares C. R. 2005, *ApJ*, in press (astro-ph/0506082)

This paper has been typeset from a $\text{\TeX}/\text{\LaTeX}$ file prepared by the author.